THE KICKER IMPEDANCE AND ITS EFFECT ON THE RCS IN J-PARC

Y. Shobuda, P. K. Saha, T. Toyama, M. Yamamoto, J-PARC Center, Ibaraki, JAPAN
Y. H. Chin and Y. Irie, KEK, Ibaraki, JAPAN

Abstract

Measurements demonstrate that the kicker impedance dominates along the RCS. Based on a newly developed theory, the impedance is measured by observing the beam-induced voltages at the ends of power cable of the kicker. Toward one mega-watt goal, it is essential to take advantage of tune manipulations and the space charge damping effect. A reduction scheme of the kicker impedance is proposed to pursue the ultimate goal at the RCS.

INTRODUCTION

There are the accelerators aiming at producing mega-watt class beams in the world [1, 2]. One of such facilities is the 3GeV rapid cycling synchrotron (RCS) in Japan Proton Accelerator Research Complex (J-PARC) [1]. In order to extract the high intensity beams from the RCS, eight distributed type kicker magnets are installed in the RCS [3].

On the other hand, in order to steadily circulate the high intensity beams in the RCS, it is important to precisely estimate the coupling impedances along the ring. In the RCS, the coupling impedance has been lowered except the kicker impedance [4]. When we apply Sacherer's formula [5], the beam should become unstable around 100 kW, where the chromaticity ξ is fully corrected in the entire energy. Accordingly, it has been concerned that the kicker impedance disturbs realizing the high intensity beam in the RCS.

Contrary to our expectation, the beam at last becomes unstable beyond about 300 kW with the fully chromaticity correction. This means that a significant gap exists between the theoretical prediction and the measurement results.

The situation has goaded us to review the estimation of the kicker impedance from theoretical and experimental points of view. In the process, the authors have found that the causality condition is not satisfied in Nassibian's formula [6, 7] describing the impedance of the kicker where all terminals are connected to the matched resistors.

Accordingly, a theory has been developed to estimate the kicker impedance. The theory describes the impedance, where the terminals of the kicker magnet are connected to the power cables [8] as well as to the matched resistors [9]. The theoretical results well reproduce the measurement results by using the standard wire-measurement scheme [10]. Moreover, the theory successfully relates the beam-induced voltages at the ends of the cables to the kicker impedance. One advantage of developing the theory is to enable to find the kicker impedance by letting a beam pass through the kicker and by measuring the beam-induced voltages at the ends of the cables.

At the same time, simulation studies have been progressing. The beam simulation code ORBIT, which is originally developed in SNS [2] for storage rings, has been upgraded by J. Holmes in order to incorporate the Lorentz-β dependence of the kicker impedance into the code. The precise estimation of the impedance brings the code into action, especially in the serious condition as in the RCS.

Before we discuss a strategy to accomplish one mega-watt beam, let us review how to produce the kicker impedance from the beam-induced voltage.

KICKER IMPEDANCE

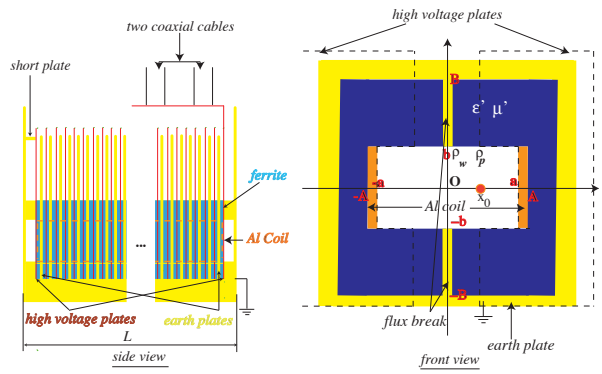

Figure 1: A schematic picture of the kicker magnet.

A schematic picture of the kicker magnet is shown in Fig. 1. The kicker magnet has four terminals at the corners. The right front and the left back terminals of the kicker are terminated by the short plates, respectively. The short plates double the excitation current by superposing the forward and backward currents, when a beam is extracted from the RCS. The right back and the left front terminals are connected to two-parallel coaxial cables, respectively.

The formulae of the kicker impedances are described as follows,

$$\begin{aligned} Z_L &= Z_L^{(0)}(x_0 = x = 0) + Z_L^{(1)}(x_0 = x = 0) \\ &+ Z_L^{(crr)}(x_0 = x = y = 0) \\ &\simeq Z_L^{(0)}(x_0 = x = 0) + Z_L^{(crr)}(x_0 = x = y = 0), \qquad (1) \\ Z_x &= \left.\frac{\partial^2 Z_L(x_0, x, y = 0)}{k\partial x_0 \partial x}\right|_{x_0 = x = 0} \\ &\simeq \left.\frac{\partial^2 Z_L^{(1)}(x_0, x, y = 0)}{k\partial x_0 \partial x} + \frac{\partial^2 Z_L^{(crr)}(x_0, x, y = 0)}{k\partial x_0 \partial x}\right|_{x_0 = x = 0}, \qquad (2) \end{aligned}$$

where Z_L and Z_x are the longitudinal and the horizontal impedances, respectively, x_0 and x are the horizontal positions of the source and the witness particles, respectively,

ISBN 978-3-95450-173-1

and k is wavenumber. The impedances $Z_L^{(0)}$ and $Z_L^{(1)}$ are approximated in low frequency region : $f < c\beta/(2\pi L)$ as

$$Z_L^{(0)}(x_0,x) = 2\sum_{m=1}^{\infty}(-(-1)^m + 1 + \cos\frac{m\pi(\rho_p+a)}{2a} - \cos\frac{m\pi(-\rho_p+a)}{2a})\frac{\sin\frac{m\pi(x+a)}{2a}}{m\pi} \times [\frac{c\beta\theta_1 Z_{c,c}(e^{j(k+\omega\theta_1)L}-1)F_3}{q(1+c\beta\theta_1)\cosh\sqrt{\frac{m^2\pi^2}{4a^2}+\omega^2\theta_1^2-k^2\beta^2}b} + \frac{c\beta\theta_1 Z_{c,c}(e^{j(k-\omega\theta_1)L}-1)F_4}{q(1-c\beta\theta_1)\cosh\sqrt{\frac{m^2\pi^2}{4a^2}+\omega^2\theta_1^2-k^2\beta^2}b} + \frac{j\omega LM_+}{\cosh\sqrt{\frac{m^2\pi^2}{4a^2}+\frac{k^2}{\gamma^2}}b}], \quad (3)$$

$$Z_L^{(1)}(x_0,x) = -2\sum_{m=1}^{\infty}(-(-1)^m - 1 + \cos\frac{m\pi(\rho_p+a)}{2a} + \cos\frac{m\pi(-\rho_p+a)}{2a})\frac{\sin\frac{m\pi(x+a)}{2a}}{m\pi} \times [\frac{\omega\theta_3 Z_{c,d}(e^{j(k+\omega\theta_3)L}-1)F_1}{q(k+\omega\theta_3)\cosh\sqrt{\frac{m^2\pi^2}{4a^2}+\omega^2\theta_3^2-k^2\beta^2}b} + \frac{\omega\theta_3 Z_{c,d}(e^{j(k-\omega\theta_3)L}-1)F_2}{q(k-\omega\theta_3)\cosh\sqrt{\frac{m^2\pi^2}{4a^2}+\omega^2\theta_3^2-k^2\beta^2}b} - \frac{j\omega LM_-}{\cosh\sqrt{\frac{m^2\pi^2}{4a^2}+\frac{k^2}{\gamma^2}}b}], \quad (4)$$

$$Z_L^{(crr)}(x_0,x,y=0) = -\frac{L_f}{a}\sum_{m=1}^{\infty}(E_m^{\gamma} - \frac{jkZ_0\tanh k_{xm}b\sin k'_{xm}(x_0+a)}{2\beta\gamma^2 k_{xm}})\sin\frac{m\pi}{2a}(x+a), \quad (5)$$

$$E_m^{\gamma} = \frac{1}{\left\{\frac{k'^2_{xm}}{k^2_{xm}} - \frac{[1-\frac{\mu' k'_{ym}\tanh k'_{ym}(b-B)\tanh k_{xm}b}{\gamma^2(1-\beta^2\epsilon'\mu')k_{xm}}]}{[1-\frac{1}{\gamma^2(1-\beta^2\epsilon'\mu')}]} \times\frac{[1-\frac{\epsilon' k'_{ym}\frac{\cosh k'_{ym}(b-B)}{\tanh k'_{ym}(b-B)}}{\gamma^2(1-\beta^2\epsilon'\mu')k_{xm}\sinh k_{xm}b}]}{[1-\frac{\mu'\epsilon'}{\gamma^2(1-\beta^2\epsilon'\mu')}]}\right\}} \times\frac{jkZ_0}{2\beta\gamma^2 k_{xm}}\left\{\frac{k'^2_{xm}\tanh k_{xm}b\sin k'_{xm}(x_0+a)}{k^2_{xm}} - \frac{(1-\frac{\mu' k'_{ym}\tanh k'_{ym}(b-B)}{\gamma^2(1-\beta^2\epsilon'\mu')k_{xm}})\frac{\sin\frac{m\pi}{2}}{\tanh k_{xm}b}}{(1-\frac{1}{\gamma^2(1-\beta^2\epsilon'\mu')})(1-\frac{\mu'\epsilon'}{\gamma^2(1-\beta^2\epsilon'\mu')})} \times[\frac{(1-\frac{\epsilon' k'_{ym}\tanh k_{xm}b}{\gamma^2(1-\beta^2\epsilon'\mu')k_{xm}\tanh k'_{ym}(b-B)})\sin k'_{xm}(x_0+a)}{\sin\frac{m\pi}{2}} - \frac{2C_r(x_0)[\cosh k'_{ym}(b-B)-1]}{k'_{ym}\sinh k'_{ym}(b-B)\cosh k_{xm}b}]\right\}, \quad (6)$$

$$M_- = \frac{(M^r(x_0)-M^l(x_0))}{2(1-c^2\beta^2(L_k-M_b)C_k)}, \quad (7)$$

$$M_+ = \frac{(M^r(x_0)+M^l(x_0))}{2(1-c^2\beta^2(L_k+M_b)C_k)}, \quad (8)$$

$$\theta_1 = \sqrt{(L_k+M_b)C_k}, \theta_3 = \sqrt{(L_k-M_b)C_k}, \quad (9)$$

$$Z_{c,d} = \sqrt{\frac{L_k-M_b}{C_k}}, Z_{c,c} = \sqrt{\frac{L_k+M_b}{C_k}}, \quad (10)$$

$$k'_{xm} = \frac{m\pi}{2a}, k_{xm} = \sqrt{k'^2_{xm}+\frac{k^2}{\gamma^2}}, \quad (11)$$

$$k'_{ym} = \sqrt{k'^2_{xm}+k^2(1-\epsilon'\mu'\beta^2)}, \quad (12)$$

$$C_r(x_0) = -\frac{1}{2(B-b)}(1-\frac{M^r(x_0)+M^l(x_0)}{L_k+M_b}), \quad (13)$$

where C_k is the capacitance per a unit length of the kicker, L_k and M_b are the self and the mutual inductances per a unit length of the coils, $M^r(x_0)$ and $M^l(x_0)$ are the induction coefficients per a unit length between the beam and the right and the left coils, respectively, β and γ is the Lorentz-β and γ, respectively, and L_f is the total length of the ferrite in the magnet. The functions $F_1(\omega), F_2(\omega), F_3(\omega)$ and $F_4(\omega)$ are obtained by solving the boundary conditions:

$$(Z_{c,d}-Z_{cable})F_1 - (Z_{c,d}+Z_{cable})F_2 - (Z_{c,c}-Z_{cable})F_3 + (Z_{c,c}+Z_{cable})F_4 = -(M_-+M_+)qc\beta - Z_{cable}qC_k c^2\beta^2(M_-+M_+), \quad (14)$$

$$-Z_{c,d}F_1 + Z_{c,d}F_2 - Z_{c,c}F_3 + Z_{c,c}F_4 = qc\beta(M_- - M_+), \quad (15)$$

$$Z_{c,d}e^{j\omega\theta_3 L}F_1 - Z_{c,d}e^{-j\omega\theta_3 L}F_2 - Z_{c,c}e^{j\omega\theta_1 L}F_3 + Z_{c,c}e^{-j\omega\theta_1 L}F_4 = -(M_-+M_+)qc\beta e^{-j\omega\frac{L}{c\beta}}, \quad (16)$$

$$-(Z_{c,d}+Z_{cable})e^{j\omega\theta_3 L}F_1 + (Z_{c,d}-Z_{cable})e^{-j\omega\theta_3 L}F_2 - (Z_{c,c}+Z_{cable})e^{j\omega\theta_1 L}F_3 + (Z_{c,c}-Z_{cable})e^{-j\omega\theta_1 L}F_4 = (M_- - M_+)qc\beta e^{-j\omega\frac{L}{c\beta}} - Z_{cable}(M_- - M_+)qC_k c^2\beta^2 e^{-j\omega\frac{L}{c\beta}}, \quad (17)$$

where

$$Z_{cable} = \frac{1}{2}\sqrt{\frac{L_{cable}}{C_{cable}}}\times [\frac{1+\frac{-\sqrt{\frac{L_{cable}}{C_{cable}}}+2R_T}{\sqrt{\frac{L_{cable}}{C_{cable}}}+2R_T}e^{-j\omega 2\sqrt{C_{cable}L_{cable}}l_{cable}}}{1+\frac{-\sqrt{\frac{L_{cable}}{C_{cable}}}+2R_T}{-\sqrt{\frac{L_{cable}}{C_{cable}}}-2R_T}e^{-j\omega 2\sqrt{C_{cable}L_{cable}}l_{cable}}}], \quad (18)$$

$$L_{cable} = \frac{R_{cable}}{j\omega} + \mathcal{L}_{cable}, C_{cable} = \frac{G}{j\omega} + C_{cable}, \quad (19)$$

$\mathcal{L}_{cable}$ is the inductance per a unit length of the cable, C_{cable} is the capacitance per a unit length of the cable, R_{cable} is the

ISBN 978-3-95450-173-1

resistivity per a unit length of the inner and outer conductors in the cable and G is the admittance per a unit length of the insulator between the conductors. Equation (18) deals with the case that two-parallel cables are connected at the end and terminated with the device having the impedance $R_T(\omega)$ (if the terminal is open as in the present kicker, R_T is identical to infinity.).

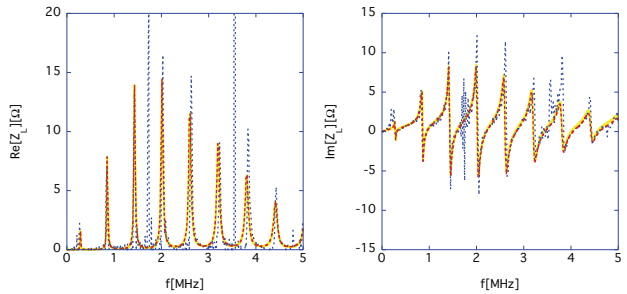

Figure 2: The theoretical (red) and the measurement (blue) results of the longitudinal impedance Z_L for $\beta = 0.54$ and the theoretical one for $\beta = 0.97$ (yellow).

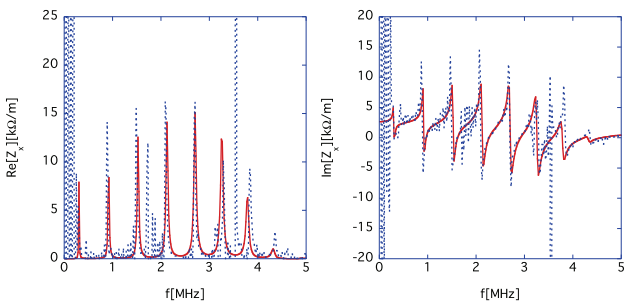

Figure 3: The theoretical (red) and the measurement (blue) results of the horizontal impedance Z_x for $\beta = 0.54$.

The impedance is theoretically calculated by solving the functions $F_1(\omega), F_2(\omega), F_3(\omega), F_4(\omega)$ in terms of the coupling factors M_- and M_+. On the other hand, the functions $F_1(\omega), F_2(\omega), F_3(\omega), F_4(\omega)$, and the coupling factors M_- and M_+ can be determined as the function of the beam-induced voltages at the ends of cables by relating the boundary conditions to those for the cables [8].

The impedances are measured by letting an injection beam from LINAC pass through the kicker once and extracting it from the RCS immediately. The theoretical and the measured results by using the beam with $\beta = 0.54$ are shown in Figs. 2 and 3. The theoretical results (red) well reproduce the measurement results (blue). The artificial sharp peaks appear in the measured results at $n/\Delta t$, where n is integer, $\Delta t (\simeq 560\text{ns})$ is the pulse length of the beam, because they are singular points in the Fourier transform of the pulse beam. The agreement between the theoretical result and the measurement one using the beam (not a wire) significantly enhances the reliability of the estimation of the kicker impedance at the RCS.

The theoretical results for $\beta = 0.97$ are shown in the yellow lines in Figs. 2 and 8, as well. The comparison between the results for $\beta = 0.54$ and the ones for $\beta = 0.97$ shows that the longitudinal impedance has little dependence on γ factor, while the horizontal one is roughly proportional to β. In general, the impedance for a non-relativistic beam tends to be smaller than that for a relativistic one. However, the longitudinal wakes are excited by the beam like cosine function [11], and they are nearly constant at low frequency during the beam passage. Consequently, the longitudinal impedance has little dependence on the γ factor at low frequency. This means that the beam tends to be more unstable horizontally than longitudinally, as it becomes relativistic.

Now, let us discuss the strategy to achieve one mega-watt goal at the RCS.

SIMULATION/MEASUREMENT RESULTS AND THE STRATEGY TO ACHIEVE ONE MEGA-WATT GOAL AT THE RCS

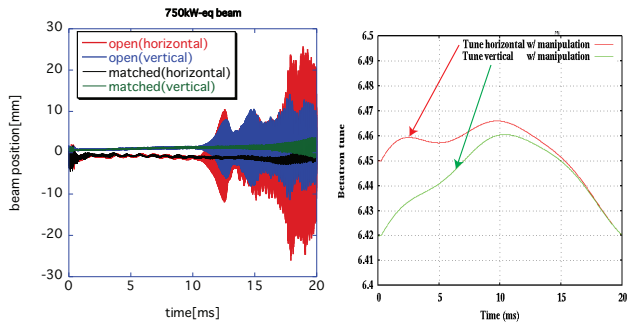

Figure 4: The left figure shows the measured beam positions of 750 kW beam for the different terminal conditions, where ξ is fully corrected in the entire energy. The right figure depicts the tune behavior in the measurements.

Let us start demonstrating that the kicker impedance dominates among the RCS impedance sources. The kicker impedance is minimized by connecting matched resistors to all terminals of the cables. The procedure eliminates the spike structures in Figs. 2 and 3 by absorbing the beam-induced current into the matched resistors [8, 12]. Figure 4 shows the measured beam positions for 750 kW equivalent beam, where the chromaticity ξ is fully corrected in the entire energy. When the terminals are open, the vertical motion (blue) becomes unstable accompanied with the horizontal motion (red), because the horizontal and vertical tunes merge during the acceleration. The black (horizontal) and green (vertical) lines demonstrate that the resistors remarkably suppress the beam growth rate, compared with the red and blue lines. Now, it is obvious that the kicker impedance substantially determines the preferable tune to increase the beam intensity.

Figure 5 shows simulation results for one mega-watt beam (the r.m.s size of momentum spread $(\Delta p/p)$ of the injection beam from LINAC is assumed to be 0.025%.). The results is obtained with the condition that the chromaticity ξ is corrected only at the injection energy. Even in the condition, the left figure predicts the beam instability, where the tunes

ISBN 978-3-95450-173-1

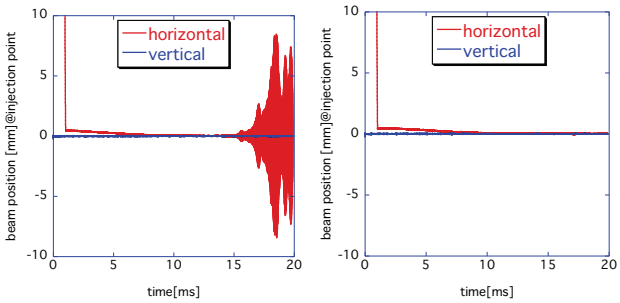

Figure 5: 1 MW simulation results, where the chromaticity ξ is corrected only at the injection energy. In the left figure, the tunes $\nu_x = 6.45$ and $\nu_y = 6.42$ are fixed during the acceleration. In the right figure, the tunes change as in the right figure of Fig. 4.

$\nu_x = 6.45$ and $\nu_y = 6.42$ are fixed during the acceleration time. Nevertheless, the right figure of Fig. 5 shows that the beam instability can be avoided, if the tunes are manipulated as in the right figure of Fig. 4.

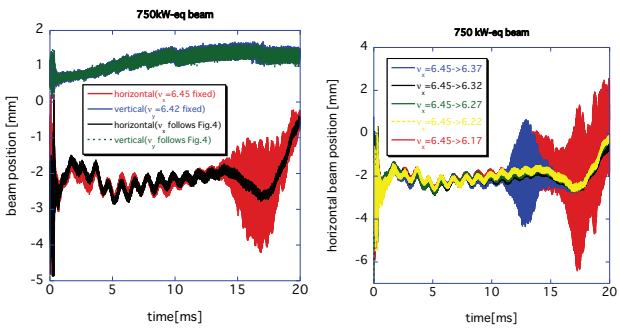

Figure 6: Measurement results of 750 kW beam, for the different tune manipulations, where the chromaticity ξ is corrected only at the injection energy.

The availability of the tune manipulation is demonstrated by using 750 kW equivalent beam and the injection beam with $\Delta p/p = 0.18\%$. In the left figure of Fig. 6, the beam instability shown by the red and the blue lines (the tunes are fixed) is stabilized to be the black and the green lines by the tune manipulation (the right figure of Fig. 4). The beam with the fixed tunes becomes unstable only in the horizontal direction, because the horizontal tune and the vertical one are isolated in the case.

Several tune manipulations are experimentally challenged by gradually decreasing the tunes toward the extraction time. The right figure of Fig. 6 shows the results. Three tracking patterns ($\nu_x = 6.32, 6.27$ and 6.22 at the extraction time) seem promising to achieve the high intensity goal.

Only tune manipulations may be insufficient to accomplish one mega-watt beam. In that case, we actively make use of the damping effect due to space charge. In the accelerator covering the intermediate energy region such as the RCS, the smaller bunching factor (average current/peak current) especially around the low energy region causes the beam stabilization by expanding the tune spread [13]. This is realized by reducing the momentum spread of the injection beam.

To demonstrate the scheme, let us prepare for the LINAC beam with two momentum spreads (0.08% and 0.18%). The left figure of Fig. 7 shows the measured bunching factor of the beams accumulating the injection beams with the different $\Delta p/p$. The injection beam with the smaller momentum spread creates the smaller bunching factors for the RCS beam. The right figure of Fig. 7 shows the corresponding RCS beam behaviors, where $\nu_x = 6.45$ and $\nu_y = 6.42$ are fixed during the acceleration, while the chromaticity ξ is corrected only at the injection energy. The beam with the smaller bunching factor is stabilized, as expected.

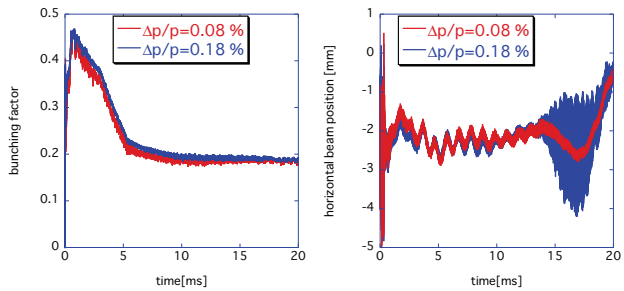

Figure 7: The measured bunching factors (left) and the horizontal beam positions for 750 kW beam (right).

In the routine operation of RCS, the sextupole magnets are turned off, and the voltage with the second harmonic RF as well as the one with the fundamental harmonic RF is excited during the injection period. In order to mitigate the space charge effect, the longitudinal painting is performed by applying the phase sweep of the second harmonic voltage (typically -100 degree) relative to the phase of the fundamental one, and by adequately superposing the voltage with second harmonic to the one with the fundamental harmonic in order that the injection beam feels momentum offset (typically -0.2 %) relative to the center of the RF-bucket (In Figs. 4-7, the phase sweep and the momentum offset are set to -100 degree and -0.2 %, respectively.).

On the other hand, the present strategy to achieve one mega-watt beam is to make maximum use of the tune manipulation combined with the space charge damping effect. When the damping effect is insufficient in reality, the bunching factor will be made lowered by activating the second harmonic voltage without the phase sweep, neither the momentum offset during the injection period.

A REDUCTION SCHEME OF THE KICKER IMPEDANCE

In order to pursue the higher intensity beam, there is no way except reducing the kicker impedance itself. In order to reduce the impedance, main idea is to insert a resistor between the coaxial cable and PFN (pulse forming network). However, the resistor has to be isolated from PFL to ensure twice excitation current due to the superposition of the forward and backward currents to extract beams, while it needs

ISBN 978-3-95450-173-1

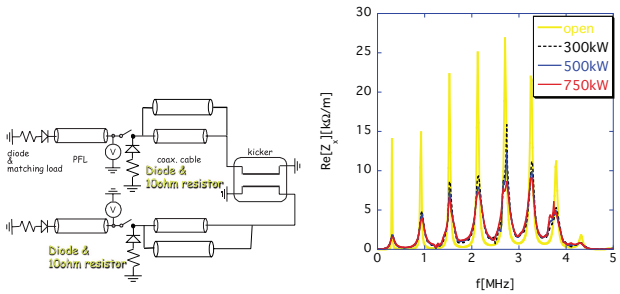

Figure 8: The terminal conditions of kicker cables (left), and the intensity dependence of the impedance at $\beta = 0.97$ (right).

to be seen by the beams to absorb the beam-induced current. A mechanism is needed to isolate the damping resistor from the pulse current from PFL. From a mechanical point of view, the easiest way is to insert a diode in front of the resistor, as in the left figure of Fig. 8.

Requirement to real diodes is that the reverse voltage V_R must have at least 40 kV or higher. The most significant concern is whether the beam-induced current flows the diode having the such high reverse voltage. In order to substantially reduce the impedance of the diode, four diodes with $V_R = 65$ kV (MD04SNKJ [14]) connected in parallel are connected to the resistor.

Now, let us observe the kicker impedance. The conventional wire method cannot measure the impedance of the kicker with the diodes. This is because the measurement is basically done in frequency domain by using weak currents with Network Analyzer.

However, it is now possible to indirectly (not directly as in sec.2) find it by measuring the behavior of R_T (of the diode plus resistor) in Eq.(18) for the high intensity beam. The results are shown in the right figure of Fig. 8. The impedance becomes lower as the beam intensity is higher, because the diode becomes more conductive for higher current and the terminal impedance R_T approaches the characteristic impedance of the kicker. The scheme successfully makes the present kicker impedance halved or less.

SUMMARY

The measured beam-induced voltage at the ends of the kicker cables is successfully transformed to the kicker impedance. The measurement enhances the reliability of the estimation of the kicker impedance, so that it is incorporated into the input of ORBIT.

In order to achieve high intensity beams, it is effective to utilize tune manipulations and the space charge damping effect. In other words, it is preferable that the momentum spread of the injection beam is as small as possible.

The measurements of the terminal impedance R_T at the ends of the kicker cables by the beam-induced voltage/current demonstrate that the kicker impedance can be halved or less by attaching the resistors combined with four diodes in parallel there.

REFERENCES

[1] http://j-parc.jp/index-e.html

[2] http://neutrons.ornl.gov/facilities/SNS/status.shtml

[3] J. Kamiya *et al*, 'Performance of extraction kicker magnet in a rapid cycling synchrotron', PRST Accel. and Beams **12**, 072401 (2009).

[4] Y. H. Chin *et al*, 'Impedance and beam instability issues at J-PARC rings', in the Proceedings of HB2008, Nashville, Tennessee, WGA01-1, (2008).

[5] B. Zotter and F. Sacherer, in *1st International School of Particle Accelerators "Ettore Majorana" - Theoretical aspects of the behaviour of beams in accelerators and storage rings* , Myrtle Hildred (ed.), 175, (1977).

[6] G. Nassibian, CERN/PS 84-25 (BR) (1984).

[7] K. Y. Ng, AIP Conference Proceedings **184**, 472 (1989).

[8] Y. Shobuda *et al*, 'Measurement scheme of kicker impedances via beam-induced voltages of coaxial cables', NIMA **713**, 11, 52-70, (2013).

[9] Y. Shobuda *et al*, 'Analytical approach to evaluate coupling impedance of traveling kicker magnets', NIMA **691**, 11, 135-151, (2012).

[10] *Handbook of Accelerator Physics and Engineering*, ed. A. W. Chao and M. Tigner (1999).

[11] A. W. Chao, *Physics of collective beam instabilities in high energy accelerators*, (Wiley, New York, 1993).

[12] Y. Shobuda *et al*, 'A trial to reduce the kicker impedance of 3-GeV RCS in J-PARC', in the Proceedings of IPAC2013, Shanghai, China, 1742, (2013).

[13] Y. Shobuda *et al*, 'Mitigation of beam instability due to space charge effects at 3GeV RCS in J-PARC', in the Proceedings of IPAC2011, San Sebastian, Spain, MOPS004, (2011).

[14] http://www.origin.co.jp/

ISBN 978-3-95450-173-1